# Estimation of Forest Fuel Load From Radar Remote Sensing

Sassan Saatchi, *Member, IEEE*, Kerry Halligan, Don G. Despain, and Robert L. Crabtree

***Abstract*—Understanding fire behavior characteristics and planning for fire management require maps showing the distribution of wildfire fuel loads at medium to fine spatial resolution across large landscapes. Radar sensors from airborne or spaceborne platforms have the potential of providing quantitative information about the forest structure and biomass components that can be readily translated to meaningful fuel load estimates for fire management. In this paper, we used multifrequency polarimetric synthetic aperture radar (SAR) imagery acquired over a large area of the Yellowstone National Park by the Airborne SAR sensor to estimate the distribution of forest biomass and canopy fuel loads. Semiempirical algorithms were developed to estimate crown and stem biomass and three major fuel load parameters, namely: 1) canopy fuel weight; 2) canopy bulk density; and 3) foliage moisture content. These estimates, when compared directly to measurements made at plot and stand levels, provided more than 70% accuracy and, when partitioned into fuel load classes, provided more than 85% accuracy. Specifically, the radar-generated fuel parameters were in good agreement with the field-based fuel measurements, resulting in coefficients of determination of $R^2 = 85$ for the canopy fuel weight, $R^2 = 0.84$ for canopy bulk density, and $R^2 = 0.78$ for the foliage biomass.**

***Index Terms*—Canopy bulk density, canopy fuel, forest biomass, polarimetric synthetic aperture radar (SAR), radar, wildfire, Yellowstone National Park (YNP).**

## I. Introduction

MAJOR ecosystems of the world (boreal forests, shrublands, grasslands, and savannas) experience recurrent fires as a result of natural causes or human activities. Statistical evidence suggests that there is an increasing trend in fire frequency and area burned from the early 1980s to the present, stimulating widespread interest in understanding fire behavior in relation to fuel characteristics and distribution [1]–[3]. When large fires cross jurisdictional boundaries, fire managers need fuel maps based on common data and mapping methods. Such maps are not often available. Remote sensing of fuel loads over large areas could aid fire management activities by providing consistent high-quality fuel maps over large areas.

Manuscript received April 14, 2006; revised August 8, 2006.

S. Saatchi is with the Jet Propulsion Laboratory, California Institute of Technology, Pasadena, CA 91109 USA (e-mail: saatchi@congo.jpl.nasa.gov).

K. Halligan is with the Department of Geography, University of California, Santa Barbara, CA 93106 USA, and also with the Yellowstone Ecological Research Center, Bozeman, MT 59718 USA.

D. G. Despain, retired, was with the U.S. Geological Survey, Bozeman, MT 59717 USA.

R. L. Crabtree is with the Yellowstone Ecological Research Center, Bozeman, MT 59718 USA.

Color versions of one or more of the figures in this paper are available online at http://ieeexplore.ieee.org.

Digital Object Identifier 10.1109/TGRS.2006.887002

In most wildfire simulations, models such as FARSITE [4], fuel variables of canopy height, canopy base height, crown bulk density, canopy biomass, and fuel load, and moisture content are important input data layers. These wildfire simulation predictions require spatial maps of fuel variables. Historically, these variables were estimated for coarse fuel model types from sparse inventory of forest structure at the stand level and from species-based algorithms at plot scale [5]. With the increased emphasis on fuel treatments across a wide range of spatial scales (local to regional) and a range of fuel types (natural habitats to urban landscapes), remote sensing technology for monitoring, measuring, and predicting the forest fuel loads has gained unprecedented importance. Currently, passive optical remote sensing from several spaceborne sensors are routinely producing information on fire occurrence, severity, burned area, and for mapping broad fuel types on regional and global scales [6]–[8], [40]. Higher-resolution multispectral or hyperspectral imagery has also been successful in determining the extent and severity of fire at local to regional scales [9], [10] and for mapping fuel moisture [41]–[44]. However, the canopy fuel characteristics that define the most important variables for predicting fire hazard and behavior cannot be readily derived from the spectral information of passive optical sensors. In recent years, there has been an increasing emphasis to use active remote sensing data such as radar and lidar sensors to estimate various components of forest structure such as crown and stem biomass, foliage water content, crown bulk density, and forest height that can be directly incorporated into fire spread models and predictions. Several studies have demonstrated the successful use of infrared scanning lidar systems to measure forest canopy structure and retrieve critical fuel parameters including canopy height, crown volume, foliage biomass, and crown bulk density [11], [45], [46]. In particular, the vertical profile of forest canopy derived from the full-wave lidar system can readily provide estimates of canopy height, canopy base height, and the distribution of foliage and branches [12]. Estimations of crown fuel variables can be obtained by using radar sensors operating at microwave frequencies with their polarimetric or interferometric measurements of forest biomass components and height [13]. Radar measurements, particularly at low frequencies (400–1500 MHz), are sensitive to crown and stem biomass and moisture content as direct measurements of biomass and structure [14]. Radar interferometric measurements are capable of providing forest height that can be readily transformed to fuel loads when combined with allometric equations available for different forest types [13]. More importantly, radar is not sensitive to visibility conditions and can be obtained day or night and through smoke and cloud cover. This makes

0196-2892/$25.00 © 2007 IEEE

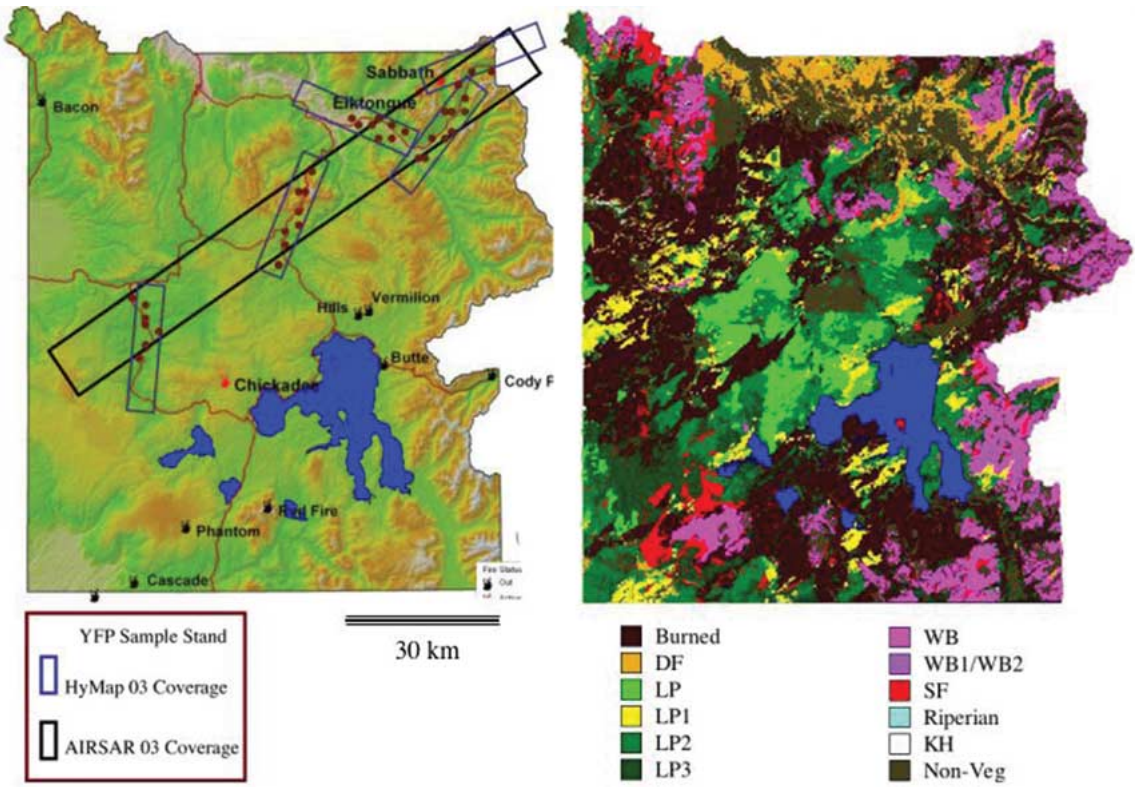


Fig. 1. YNP. (left) AIRSAR coverage and location of sample stands (HyMap03 was acquired along with AIRSAR but never used in this paper). (right) Vegetation cover map derived from ecosystem map [15]. The vegetation and fuel types are LP, LP1, LP2, and LP3 for climax and four successional stages of lodgepole pine, DF for douglas fir, WB, WB1, and WB2 for climax and two postdisturbance successional stages of whitebark pine, SF for Engelmann spruce and subalpine fir, Riperian type for herbaceous and sagebrush, KH for krummholz zone, and non-veg and rocky and geyser surfaces, and burned for recent burned areas with dead trees or early successional stages.

spaceborne radar remote sensing an important technique for global monitoring and managing forest fire.

In this paper, we concentrate on the use of high-resolution synthetic aperture radar (SAR) sensors to develop the spatial distribution of fuel loads for fire management in the Yellowstone National Park (YNP). By developing algorithms for estimating biomass components and forest structure from airborne polarimetric SAR measurements, we demonstrate the capability of radar systems for the global monitoring of forest fuel and potential tools for forest fire management. Currently, several airborne sensors such as NASA's Airborne SAR (AIRSAR) system, the GeoSAR interferometric sensor, and commercial sensors such as the AeS-1 from Intermap Technologies Corporation are available for local to regional mapping of forest fuel. These sensor technologies have the potential of being deployed in future NASA or international earth observing platforms to improve the monitoring and management of wildland fuels on a global scale.

## II. Study Area

We chose YNP as our study site for several reasons (Fig. 1). 1) The park contains a variety of fuel types common to the Northern Rocky Mountains region consisting predominantly of coniferous forests and sagebrush shrublands [15], [16]. 2) The ecology of forest fire and postfire successional history have been well documented [16], [17]. The park has been maintained as a protected area since 1872, limiting human impact and development in the region. 3) A large archive of field, aerial photography, geographical information system (GIS), and remote sensing data is available for comparison and validation studies [18], [19], [47].

YNP covers an area of approximately 899 500 ha surrounded by seven national forests in three different states (Wyoming, Montana, and Idaho). It consists of large volcanic plateaus of rhyolitic rocks surrounded by mountains of predominantly andesitic rocks, with varying soil fertility and water holding capacity, and a rough terrain varying in elevation from approximately 1800 to 3800 m. Severe droughts, various management approaches, and large-scale fires have contributed to the ecological evolution and vegetation patterns of the park since its establishment in 1872. The high relief terrain of the park provides unique challenges to fire fighters and fire managers and similar difficulties for mapping fuel loads for GIS and remote sensing experts. Existing vegetation and fuel maps are based on different criteria and with variable degrees of reliability, creating a new incentive for developing a common fuel map to effectively manage cross-boundary fire events. Approximately 83% of the total forested area of YNP is dominated by lodgepole pine (*Pinus contorta* var. *latifolia*) ranging in age up to 300–400 years [15]. The lodgepole pine forest occurs as a mosaic of successional stages on extensive gently rolling plateaus with limited variations in tree species, particularly mixtures of coniferous and deciduous trees. Canopy tree density

ranges from 250 to 1000 trees/ha and reaches approximately 25 m tall. Crown biomass ranges around 20–40 Mg/ha. Understory trees are generally sparse, and fine surface fuels are light, consisting mostly of grouse whortleberry (*Vaccinium scoparium*) approximately 20–30 cm tall. Sagebrush (*Artemisia tridentata*) stands with fuel loads of approximately 0.5–0.7 kg/m$^2$ are a minor component and include pockets of wet marshes and dry to mesic grasslands.

Existing maps such as that shown in Fig. 1 provide information about vegetation types, successional stages, and disturbance history. Cover types are named for their dominant canopy followed by a ranked value indicating the successional stage. For example, lodgepole pine cover types include, in increasing progress from disturbance toward climax, LP0, LP1, LP2, and LP3. LP0 stands are those that occur following a stand replacing disturbance, such as crown fire until the time of canopy closure, which often occurs at about 40–50 years in YNP. LP3 stands represent a subclimax stand leading to a spruce-fir climax [15]. These maps are based on detailed interpretation of aerial photography surveys and extensive field measurements and are used for wildfire management [15]. However, they are mostly created more than 20 decades ago, and the process of reproducing them is labor intensive and cannot be done frequently.

## III. Field Data

Field data for this paper were collected between June and September of 2002 and 2003 by a team of trained field personnel. A total of 833 plots were sampled in 64 vegetated stands across a range of vegetation types and disturbance histories in YNP. Stand boundaries were delineated using interpretation of remote sensing images, and sampling areas between 5 and 10 ha were selected based on how well they represent the vegetation types and fire histories in the park, their coverage by remote sensing data, and logistical considerations for field sampling. A forest stand is defined as a sampling area with uniform distribution of trees and species and representative of larger YNP vegetation and fuel types. An average of 12 sample plots was located within each stand using a regular grid where the spacing between plots varies from stand to stand. Distances between plots ranged from 50 to 75 m based on stand size and shape but were consistent within a given stand. The use of a regular grid design maximized the sampling efficiency while ensuring unbiased plot location. All plots were geolocated using Trimble Geoexplorer II geographic positioning system (GPS) units. Vegetation sampling methods were designed to be compatible with existing fuel sampling protocols for inventorying weight of forest floor duff, forest floor litter, herbaceous vegetation, shrubs, small conifers ($< 3.05$ m high), and downed woody material [22]. This method was modified slightly and expanded to include procedures for measuring mature trees as well as additional measurements on herbaceous vegetation and shrubs. Plot basal area was measured using a 2.5-m$^2$ basal area factor forestry prism. Vegetation type was described with regards to habitat type and cover type following Despain [15]. At each plot, the following parameters were recorded: habitat type, cover type, average duff depth, and GPS locations. The GPS locations were accurate within a few meters (less than 10 m), allowing extraction of remote sensing data from plot locations with relatively high accuracy. Percent canopy cover was measured using a handheld spherical densitometer. For mature trees, diameter at breast height (DBH) at 1.3 m from ground, species, live/dead, and height to the top and base of live crown were measured for each tree counted by the prism method. The plots established by the prism were circular and variable in radius. Downed wood in three size categories was measured along a line transect. The average height and stem count were recorded for all species of shrubs found on 1-m$^2$ microplots. For herbaceous vegetation, the biomass of live vegetation and litter was measured on the highest biomass microplot (clipped, dried, and weighed) and estimated as a percent of the standard on other microplots, and the vegetation height and digital photos were recorded.

TABLE I
AIRSAR System Parameters Used in Data Acquisition Over the YNP in July 2003

| AIRSAR/TOPSAR System Parameters | |
|---|---|
| Radar Parameter | Value |
| Frequency Polarimetric | L-band (1.26 GHz), P-band (0.45 GHz) |
| Frequency Interferometry | C-band (5.3 GHz) |
| Range Bandwidth | 40 MHz (L, and C-band), 20 MHz(P-band) |
| Peak Transmit Power | 1 kW (P) , 6 kW (L), 2 kW (C) |
| Baseline Length | Short (2.5 m), Long (5.0 m) |
| Baseline Angle relative to Horizontal | $62.8^0$ |
| Operating altitude | 9.5 km |
| Incidence Angle | $28^0$-$63^0$ |
| Slant range near/far | 8.9/17.3 km |
| Range and Azimuth Pixel-Spacing | C-band (5 m), L-band (5 m), P-band (10 m) |
| Processed Ground Range Swath | 11.3 km |

Field data for each of the 833 sample plots were entered into a database and checked for errors. Allometric equations from Brown *et al.* [22] and Van Hooser and Chojnacky [23] were used to calculate plot and stand-level fuel loads and live biomass. Live biomass for trees was separated into stem and crown components, with crown components further divided into diameter size classes commonly used for fuel assessments: 0–0.25 in (0.25–0.6 cm), 0.25–1 in (0.6–2.5 cm), 1–3 in (2.5–7.6 cm), and greater than 3 in ($> 7.6$ cm). Live biomass was calculated per sample and then aggregated up to the plot and stand levels for comparison with remote sensing data.

## IV. Remote Sensing Data

In July 2003, the NASA Jet Propulsion Laboratory AIRSAR system on the NASA DC-8 aircraft acquired polarimetric images along with simultaneous interferometric topographic SAR (TOPSAR) data over YNP. The entire YNP was covered in a mosaic mode with north–south strips 15 km wide at 10-m spatial resolution. In addition, a diagonal flight line with 233° heading in the northeast to southwest direction at 5-m resolution (Table I) was acquired as part of a multisensor campaign (including hyperspectral and lidar sensors). The AIRSAR was operating at P-band (435 MHz, 20-MHz bandwidth, 10-m

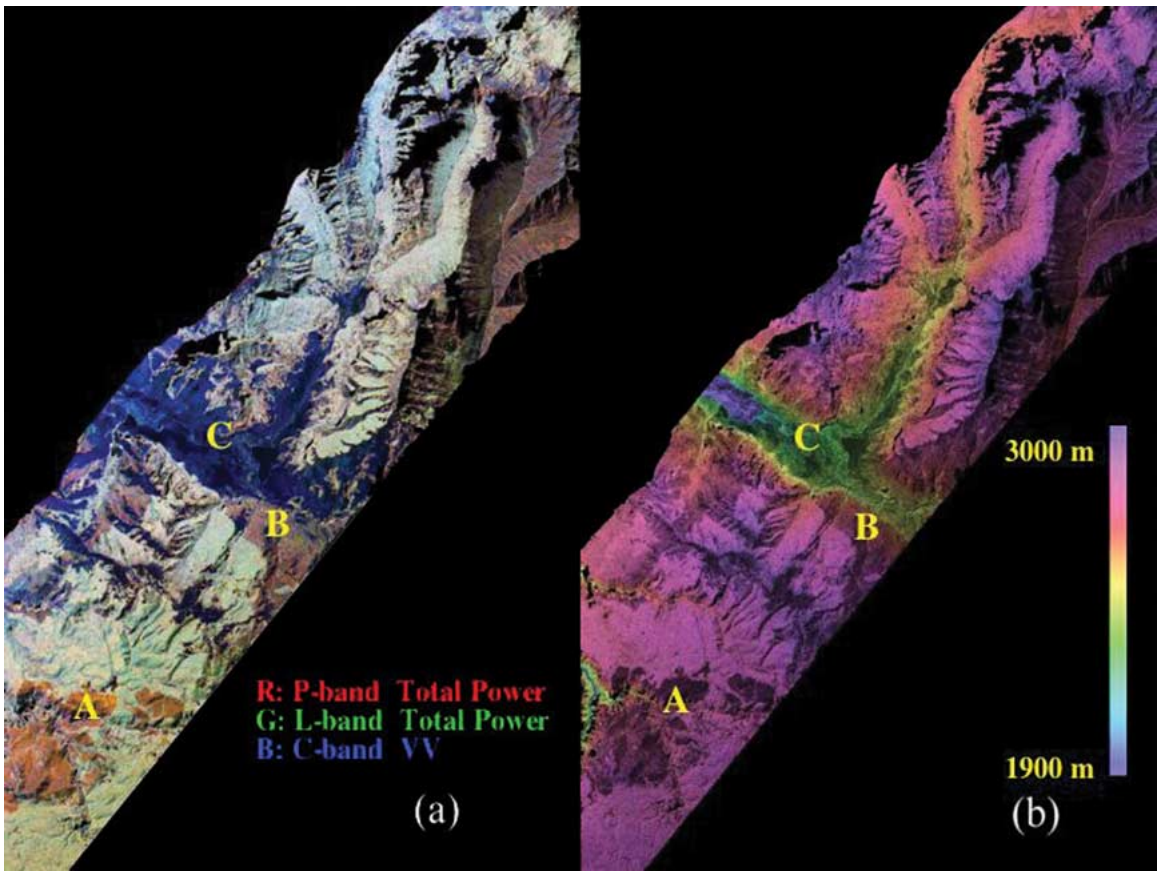


Fig. 2. Sample of AIRSAR imagery acquired over the northeastern section of YNP in July 2003 with three-band polarimetric data on the left and the digital elevation image on the right. Locations A and B in the images denote burn scars from the 1994 and 1988 fires, respectively. Location C denotes an area of sagebrush/grassland vegetation in the Lamar River valley.

resolution), L-band (1.25 GHz, 40-MHz bandwidth, 5-m resolution) in fully polarimetric modes, and C-band (5.3 GHz, 40-MHz bandwidth, 5-m resolution) at vertical polarization (VV) and interferometric mode. The images have a swath width of approximately 10 km with incidence angles ranging from about 28° to 63° with approximately 45° at the center of the swath. Fig. 2 shows a short section of the high-resolution AIRSAR data used in this paper over the Lamar River valley in the northeastern section of the park. All images were terrain corrected using the digital elevation data acquired by the TOPSAR interferometric modes [32], [48]. The images were orthorectified in a Universal Transverse Mercator projection using the Landsat Enhanced Thematic Mapper data (15-m resolution) with a large number of ground control points (123 points) that provided a registration accuracy of approximately 25 m (five pixels). For all data analysis and algorithm development in the next sections, we resampled SAR images to their lowest common resolution of P-band data (10 m).

## V. Methods

### A. Estimation of Forest Biomass Components

Estimation of forest biomass from radar data is possible due to the physical relationship between radar backscatter measurements and forest structure and biomass components. The backscatter signal at linear polarizations (HH, HV, VV; horizontal (H) and vertical (V) for transmit and receive configurations, respectively) is sensitive to those structural components that can resonate with the radar wavelength. At the same time, a strong backscatter (above noise level) results from objects with reasonable moisture content. In other words, depending on the wavelength of the measurements, the radar return from a forest can be related to scattering from live stems, branches, and foliage based upon their abundance and moisture content within a resolution cell. In most forest types, successional stages translate into differences in structural parameters such as tree size, density, and biomass components. These parameters are directly related to fuel loads in the forest canopy that are normally consumed in crown fires such as live and dead foliage, lichen, and fine live and dead branchwood [5]. Furthermore, as forest fuels are modeled based on the amount of vegetation biomass components, radar measurements can provide the most direct estimates of forest fuels.

There are two approaches for estimating the forest parameters, namely: 1) the statistical approach (e.g., regression analysis) and 2) the inversion of physically based backscatter models. The statistical approach is based on the correlation of radar backscatter measurements at different frequencies and polarizations with forest structure and biomass components obtained from field measurements [24], [25]. By separating regression models based on forest type and landscape features (topography), we can improve the accuracy of biomass

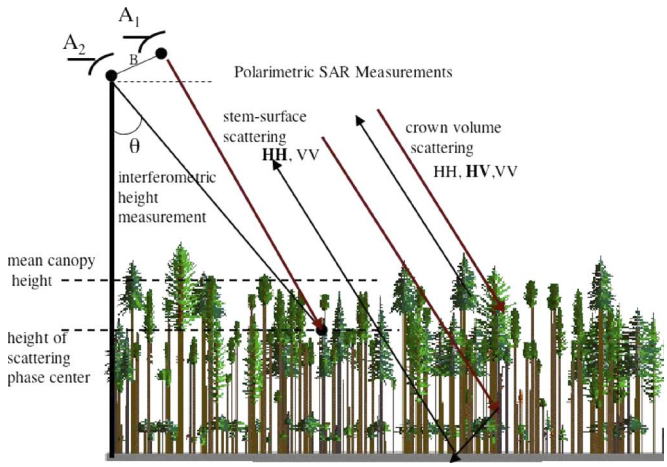


Fig. 3. SAR polarimetric and interferometric measurements of a typical forest over flat landscape, with dominant polarizations contributing to crown and stem-surface scattering mechanisms, and interferometric measurement of the height of the scattering phase center as the height of an equivalent scatterer representing the collection of scatterers within a pixel.

estimation [14]. The estimation of forest structural parameters from physically based models, on the other hand, requires inversion techniques such as the semiempirical approach [14], a parametric approach [26], or the use of the neural network training approach [27], [28].

Radar backscatter measurement from a forest stand includes several scattering mechanisms, as shown in Fig. 3. In general, the scattering mechanisms are of the form

$$\begin{aligned}\sigma^0 &= \sigma^0_{\rm gr} + \sigma^0_{\rm veg}\\ \sigma^0_{\rm gr} &= (1-\eta)\sigma^0_s + \eta\sigma^0_s e^{-\beta W}\\ \sigma^0_{\rm veg} &= \eta\sigma^0_v(1-e^{-\beta W}) + \eta\sigma^0_{\rm vs}e^{-\beta W}\end{aligned} \quad (1)$$

where $\eta$ is the fraction of the area filled by the forest canopy, $e^{-\beta W}$ is the vegetation transmitivity with $\beta$ as the two-way attenuation in the forest, and $W$ is the biomass assuming 100% dry weight. The series of equations given in (1) simplifies a more complex backscattering model with different scattering mechanisms [14], [29], [30]. The uppermost equation divides the total backscatter $\sigma^0$ into ground $\sigma^0_{\rm gr}$ and vegetation $\sigma^0_{\rm veg}$ contributions. The ground term includes the direct ground scattering from the surface $\sigma^0_s$ weighed by the coefficient $(1-\eta)$ and a second term that represents the surface scattering under the vegetation canopy. The vegetation contribution is given by the last equation and includes both direct volume scattering $\sigma^0_v$ and volume–surface $\sigma^0_{\rm vs}$ interaction term. The volume scattering $\sigma^0_v$ and volume–surface $\sigma^0_{\rm vs}$ (double-bounce) scattering cross sections are both a function of vegetation water content and biomass. Note that, for simplicity, we have considered the forest as one layer and have suppressed the subscripts showing the transmitted and received polarization coefficients. By including the wave polarizations in the above equations, all terms except the biomass $(W)$ and the fraction of forest cover $\eta$ will be different. In other words, polarimetric radar backscattering can provide independent measurements of forest structure and biomass.

From (1), it is clear that the estimation of the aboveground biomass from a physically based model requires several assumptions about the forest or a simplification of the model into a parametric form [14], [26]. In this paper, we start by prescribing a general statistical regression model that relates the biomass components to radar backscatter measurements. This model has a quadratic form to approximately mimic the loss of sensitivity of radar backscatter at higher biomass values. By replacing $W$ by its natural logarithm $\log(W)$ and the backscatter coefficients in decibels as $10\log(\sigma^0)$, the general form of the regression model can be written as

$$\begin{aligned}\log(W) = a_0 + a_1\sigma^0_{\rm HV} + a_2\left(\sigma^0_{\rm HV}\right)^2 + b_1\sigma^0_{\rm HH}\\ + b_2\left(\sigma^0_{\rm HH}\right)^2 + c_1\sigma^0_{\rm VV} + c_2\left(\sigma^0_{\rm VV}\right)^2\end{aligned} \quad (2)$$

where $W$ is the total aboveground biomass or its components (stem, branch, and foliage), and $\sigma^0_{\rm HV}$, $\sigma^0_{\rm HH}$, and $\sigma^0_{\rm VV}$, respectively, represent the radar backscatter measurements at three transmit and receive polarization configurations [31]. Equation (2) can be considered a parametric equation including all scattering mechanisms represented by the radar polarimetric measurements [26]. The form of (2) as a second-order polynomial can be readily expected from (1) after substitution of $W$ with $\log(W)$ and the expansion of each term in $\log(W)$. Therefore, (2) can be referred to as a semi-empirical algorithm for estimating forest biomass components.

To customize (2) for our application over YNP, we first divide the forest biomass into crown and stem components and then include the effect of surface topography on changing the scattering mechanisms. The following equations were used as the basis of the semiempirical model for crown and stem biomass estimation:

$$\begin{aligned}\log(W_c) = a_0 + a_1\sigma^0_{\rm HV}\cos(\theta_0-\theta_l) + a_2\left(\sigma^0_{\rm HV}\cos(\theta_0-\theta_l)\right)^2\\ + b_1\sigma^0_{\rm HH}\sin(\theta_0-\theta_l) + b_2\left(\sigma^0_{\rm HH}\sin(\theta_0-\theta_l)\right)^2\\ + c_1\sigma^0_{\rm VV}\cos(\theta_0-\theta_l) + c_2\left(\sigma^0_{\rm VV}\cos(\theta_0-\theta_l)\right)^2\end{aligned} \quad (3)$$

$$\begin{aligned}\log(W_s) = a_0 + a_1\sigma^0_{\rm HV}\sin(\theta_0-\theta_l) + a_2\left(\sigma^0_{\rm HV}\sin(\theta_0-\theta_l)\right)^2\\ + b_1\sigma^0_{\rm HH}\cos(\theta_0-\theta_l) + b_2\left(\sigma^0_{\rm HH}\cos(\theta_0-\theta_l)\right)^2\\ + c_1\sigma^0_{\rm VV}\cos(\theta_0-\theta_l) + c_2\left(\sigma^0_{\rm VV}\cos(\theta_0-\theta_l)\right)^2\end{aligned} \quad (4)$$

where $W_c$ and $W_s$ are, respectively, the crown and stem biomass, and the angles $\theta_0$ and $\theta_l$ are the incidence angle of the SAR platform at the center of the image pixel and the local incidence angle at the same location. When $\theta_0$ and $\theta_l$ are equal, the surface has no topography, and the biomass is estimated from those terms representing the dominant scattering mechanism of forest over a flat surface [32]. The local incidence angle is calculated in terms of surface slope and aspect angles as

$$\cos\,\theta_l = \sin\,\alpha\,\sin\,\theta_0\cos(\beta-\beta_s) + \cos\,\alpha\,\cos\,\theta_0 \quad (5)$$

where $\alpha$ is the local slope, $\beta$ is the azimuth angle of the radar illumination direction, and $\beta_{\rm s}$ is the aspect angle at the local slope [32]. Given the geometry of SAR platform and the topographic data acquired by AIRSAR C-band interferometry, the local incidence angle for any pixel location can be calculated from (5).

We used (3) and (4) to estimate the crown and stem biomass. Here, by biomass, we refer to dry weight per unit area of

forest component. However, depending on the type of field data used to estimate the unknown coefficients in (3) and (4) , the definition can be changed to forest water content or wet biomass. The first step is to develop training and test data sets to estimate the unknown coefficients and to assess the accuracy of the estimation. There were 623 plots within the area covered by radar images. We extracted backscattering coefficients from an area of 5 $\times$ 5 pixels centered at plot locations. The average backscatter represented an area of 25 $\times$ 25 m that was slightly larger than the average plot size. The data had better quality than the single pixel values because of the reduced errors due to the misregistration and the speckle noise (450 looks at L-band and 225 looks at P-band).

To develop training and test data sets, we used a combination of bootstrapping and holdout procedures to randomly split the plot data into training and testing subsamples [34]. The training data were used to estimate the coefficients of (3) and (4), respectively, for the stem and crown biomass, and the test data were used to evaluate the accuracy of the estimation. The estimation was performed using a least-squared second-order polynomial fit to the data with the singular value decomposition procedure [49]. Once the coefficients were estimated, the resulting equation was evaluated using the testing subsample, and the correlations between predicted and measured values were computed using Spearman's rank correlation coefficients. The inclusion of the bootstrapping technique provided an additional nonparametric procedure for including sampling variability in predicting the expected accuracy of the estimation procedure. In the bootstrap method, the holdout approach is repeated many times by replacing the training and test data with a new random split to the initial plot data. The procedure was repeated several times to come up with an optimum algorithm (with highest estimation accuracy) and an unbiased accuracy assessment of biomass estimation [33], [34]. Since the bootstrapping iteration approach was performed using a random sampling technique, the optimum algorithm was obtained by simply choosing the best algorithm out of all randomly developed algorithms. The iterations were performed 25 times, which provided sufficient sampling to reach the Monte Carlo estimation of the accuracy [34]. The estimation and evaluation program was written in interactive data language and included the necessary statistical and estimation routines.

### *B. Estimation of Fire Fuel Parameters*

Fire fuels are defined as the aboveground organic biomass components that can contribute to wildland fire. They can be divided into live or dead, woody or herbaceous, and into different size categories. In general, there are two main types of wildland fires, namely: 1) surface and 2) crown fires [5]. Surface fire is the combustion of the fuel layer within or immediately above the ground surface and below the canopy (generally less than 2 m in height). Surface fuels consist of organic material in the soil, needles and leaves, grass and other herbaceous and shrubby vegetation, tree seedlings, and dead and down branch wood and logs on or near the soil surface [22]. Crown fire, on the other hand, is the combustion of the elevated canopy fuel consisting of live and dead foliage, lichen, and fine live and dead branchwood. Crown fuels often have higher moisture content and lower bulk density than surface fuels. Crown fires are intense and fast moving, with their spread depending primarily on a physical situation including the quantity and arrangement of fuels, topography, and weather. Remote sensing technologies image vegetation canopies and are capable of measuring the crown fuel characteristics including fuel loads and moisture. Surface fuel characteristics, on the other hand, are often obscured by canopy vegetation, limiting their ability to be directly derived from remote sensing data. Instead, surface fuels are either estimated through their correlation with canopy fuels or extrapolated from field measurements. Crown fuel characteristics are defined in terms of several parameters such as canopy fuel weight, crown bulk density, canopy cover, foliage moisture content, canopy base height, and canopy height [5]. Among these, we focused on three parameters in this paper.

1) Canopy fuel weight is defined as the biomass of the canopy including foliage and thin branchwood and is often computed for forest tree species using allometric equations [21], [23]. These equations are developed from field data and are capable of separating foliage and branch biomass using measured structural variables such as tree DBH, tree height, and crown ratio. The biomass of small branches is associated with several classes of fuel loads. In particular, variables such as 1-h and 10-h branchwood fuels representing the biomass of 0–1- and 1–3-cm branchwoods are derived from similar allometric equations. Alternative approaches to allometric equations are leaf area index measurements [35] and radar-based crown biomass estimation [14]. In this paper, we developed canopy fuel weight from the radar data.
2) Crown bulk density is defined as the mass of available canopy fuel per unit canopy volume and is an important parameter to predict both the crown fire initiation and the spread. However, it is a difficult parameter to measure in the field. For stands where the canopy biomass is assumed to be uniformly distributed along the canopy height, this parameter can be computed as the available canopy fuel load or biomass divided by canopy height. However, in general, for complex canopy structures, it is obtained from stand inventory data [36]. Knowing the canopy vertical profile, the bulk density can be defined as the running mean of the canopy density for layers 0.3 m thick with uniform canopy distribution. Remote sensing measurements such as the lidar full-wave vertical profile or radar interferometric measurements can be converted into the crown bulk density [11], [13]. In this paper, we estimated the crown bulk density from the field-measured forest structure using the relationship

$$\mathrm{CBD} = W_c/(H_t - H_{\mathrm{blc}}) \tag{6}$$

where CBD is the effective crown bulk density assuming a uniform vertical distribution of canopy, $W_c$ is the total canopy weight (live and dead), $H_t$ is the average height of the canopy, and $H_{\mathrm{blc}}$ is the average height to base of the live crown of all trees in a plot. After computing the bulk density from the structural data measured at the plot level,

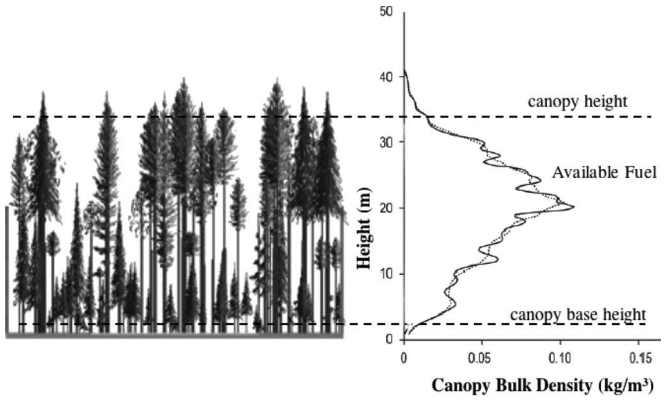


Fig. 4. Vertical profile of available fuel in terms of canopy bulk density in a near climax LP3 or spruce-fir forests in YNP. Canopy mean height and canopy base heights are shown in terms of bulk density values of 0.011 kg/m$^3$.

we used a regression model between CBD and the crown and stem live biomass to convert the radar-measured biomass components to crown bulk density (Fig. 4).

3) Foliage biomass is an important parameter used in fire fuel models with more influence on fire spread than initiation [5]. For a given set of environmental conditions, moisture content and biomass of conifers vary among species and on a seasonal temporal scale. There is little observed variation in these parameters on a daily or even weekly temporal scale, although annual patterns can be seen during times of extreme conditions such as drought. Several studies in North America have contributed to developing allometric equations for foliage moisture content and tabulating values for different tree species [5], [50], [51]. In general, for old foliage (needles from previous years), the values for moisture content can vary from low values of approximately 80% of the dry weight in severe late summer drought to high values of less than 125% in the spring. New growth of the current year starts at about 250%–300% in late June and dries to about 130% by late August. A default average value of 100% is a useful working number for late summer when fires are most likely to burn large acreages. The 100% moisture content assumes that half of the live foliage mass is due to water. Foliage biomass and moisture content can also be obtained directly from radar remote sensing [14], [24], [26] or from optical remote sensing data [37], [42], [44], [45]. In this paper, we did not measure the foliage moisture content in the field and hence do not have data for the development and validation of radar-derived moisture content [26]. However, by assuming 100% moisture content as the mean moisture for all foliage types in the study areas at the time of the AIRSAR data acquisition (mid to late summer), the foliage biomass was assumed to be equal to the total foliage water content. We used the field-derived relationship between the total canopy biomass and the live foliage biomass to convert the radar measurements to the distribution of foliage dry biomass over the study area. The overall procedure for estimating the canopy fuel parameters from SAR data is shown in the flowchart provided in Fig. 5 and discussed in the following sections.

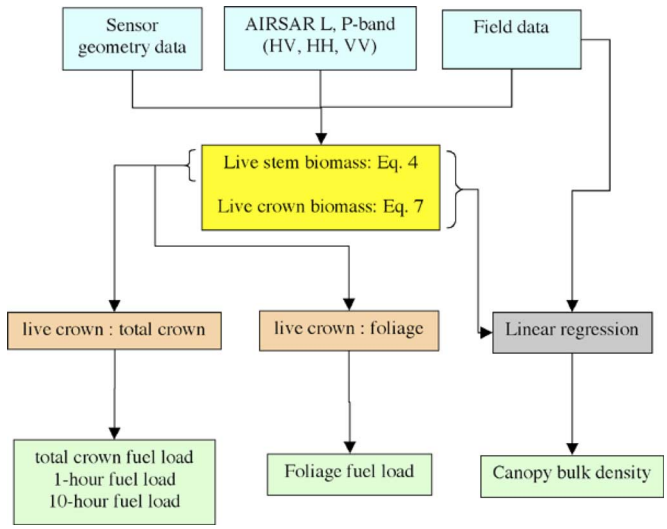


Fig. 5. Flowchart summarizing the methodology to derive fuel variables from combining SAR measurements and field data.

## VI. Results

### A. Radar Sensitivity to Aboveground Biomass

We started the analysis by examining the sensitivity of the radar backscatter measurements at L-band and P-band to the total aboveground live biomass (AGLB). We used six SAR images, two frequencies (L-band and P-band), three polarizations (HH, HV, and VV) at 10-m spatial resolution, and extracted backscattering coefficients from 427 plots from 42 forest stands. The relations between polarized backscatter and log (AGLB) are shown in Fig. 6. The regression coefficients $(R^2)$ were obtained by fitting a second-order polynomial to the backscatter data at each polarization. The second-order polynomial provided a better fit to the data than the linear regression model and was better suited to represent the saturation of radar signal at higher biomass values. For the P-band-polarized backscatter measurements, $R^2$ values were 0.61, 0.69, and 0.49, respectively, for PHH, PHV, and PVV. For L-band measurements, $R^2$ values were 0.50, 0.42, and 0.57, respectively, for LHH, LHV, and LVV. The spread in the data depends on several factors. First, the small size of the forest plots and the errors in geolocation can often cause errors in extracting the exact backscatter values. Second, speckle in high-resolution radar imagery can introduce variations in backscatter measurements over forests with similar AGLB values. Finally, depending on the canopy architecture (branch and leaf orientation), canopy moisture content, spatial distribution of trees, soil roughness and moisture, and topography, the backscattering coefficients may vary for forests with similar AGLB. Moreover, the errors associated with the field data and allometric equations also contribute to the variations shown in backscatter plots. The AGLB values range from 3 Mg/ha for early successional forests to 347 Mg/ha for mature forests. The sensitivity of radar backscatter to biomass decreases for high biomass density, starting to level at AGLB values greater than 200 Mg/ha for P-band channels and greater than 100 Mg/ha for L-band channels. However, the low sensitivity of radar to high biomass, the so-called saturation region, is different for copolarized and

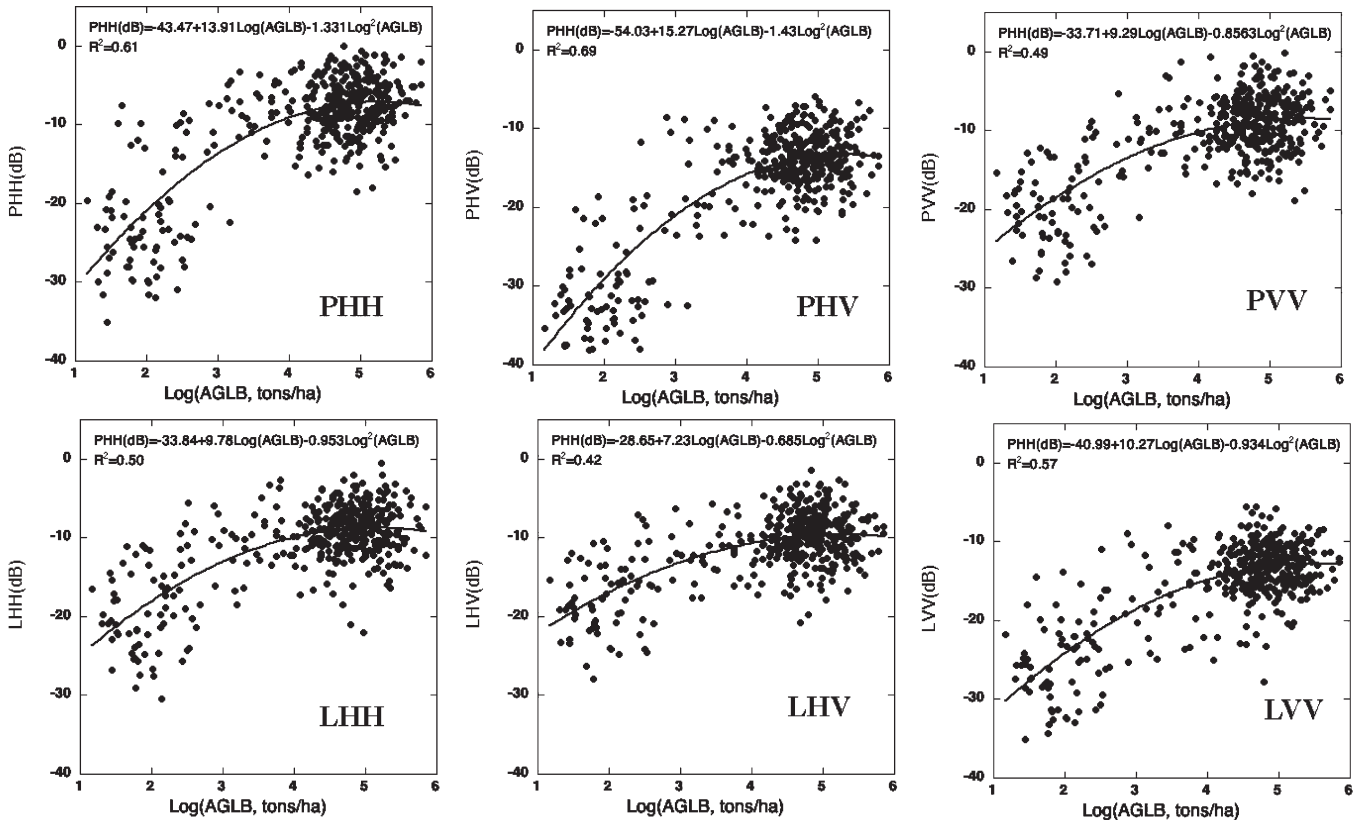


Fig. 6. Backscattering coefficient at linear polarization combinations versus the natural logarithm of field-measured AGLB for 427 forest plots. The regression coefficients were found by fitting a quadratic equation to the data.

TABLE II
REGRESSION MODELS SUMMARIZING THE RELATIONSHIP OF THE SAR POLARIMETRIC BACKSCATTER MEASUREMENTS IN DECIBELS WITH THE NATURAL LOGARITHM OF THE AGLB IN MEGAGRAMS PER HECTARE

| | |
|---|---|
| **Plot Level Data** | |
| $LHH(dB) = -33.84 + 9.78Log(AGLB) - 0.953(Log(AGLB))^2$, | $R^2 = 0.50$ |
| $LHV(dB) = -28.65 + 7.23Log(AGLB) - 0.685(\log(AGLB))^2$, | $R^2 = 0.42$ |
| $LVV(dB) = -40.99 + 10.27Log(AGLB) - 0.934(Log(AGLB))^2$, | $R^2 = 0.57$ |
| $PHH(dB) = -43.47 + 13.91Log(AGLB) - 1.331(Log(AGLB))^2$, | $R^2 = 0.61$ |
| $PHV(dB) = -54.03 + 15.27Log(AGLB) - 1.43(\log(AGLB))^2$, | $R^2 = 0.69$ |
| $PVV(dB) = -33.71 + 9.29Log(AGLB) - 0.856(Log(AGLB))^2$, | $R^2 = 0.49$ |
| **Stand Level Data** | |
| $LHH(dB) = -21.97 + 2.542Log(AGLB)$, | $R^2 = 0.56$ |
| $LHV(dB) = -29.00 + 3.105Log(AGLB)$, | $R^2 = 0.71$ |
| $LVV(dB) = -19.36 + 1.837Log(AGLB)$, | $R^2 = 0.48$ |
| $PHH(dB) = -26.09 + 3.771Log(AGLB)$, | $R^2 = 0.81$ |
| $PHV(dB) = -35.01 + 4.296Log(AGLB)$, | $R^2 = 0.88$ |
| $PVV(dB) = -21.89 + 2.652Log(AGLB)$, | $R^2 = 0.83$ |

cross-polarized backscatter and depends on a variety of forest and surface parameters discussed earlier.

The relations shown in Fig. 6 and repeated in Table II also indicate that the polarized backscattering measurements provide different information about the forest structure and biomass and suggest that optimal approaches estimating biomass might combine all measurements as shown in (2)–(4). Another way of looking at the sensitivity of the radar backscatter to biomass is to include a larger range of biomass from very low vegetation to dense old growth forests. By extracting the radar backscatter for polygons over all 64 stands where the inventory plots were established (including early successional and sagebrush sites), new plots for L-band and P-band backscatter were generated (Fig. 7). In these plots, the errors associated with misregistration and speckle noise were reduced as each stand polygon includes a large number of 10-m pixels (more than 100). The sensitivity and the dynamic range of the backscatter measurements with respect to log (AGLB) improved, resulting in values for $R^2$ of 0.81, 0.88, and 0.83 for PHH, PHV, and PVV, and 0.56, 0.71, and 0.45 for LHH, LHV, and LVV, respectively. A linear regression provided the best fit to the data as the stand numbers were limited and represented mainly the low and high values.

Both plot and stand-level backscatter show higher sensitivity to aboveground biomass from the P-band data. The L-band backscatter data show less variations and better sensitivity for low biomass values. By examining the sensitivity of radar to aboveground biomass, we concluded that including plots or stand data from a lower range of biomass improves the correlations between backscatter and biomass and would improve the development of the estimation algorithm. This approach has been common in remote sensing data analysis, in particular in radar and lidar estimation of forest structure and biomass [11], [24], [38], [39]. By including a larger range of biomass values in the data analysis, the dynamic range of measurements is increased in comparison with the natural variations in the data caused by other structural and environmental variables, especially in the high end of the biomass values.

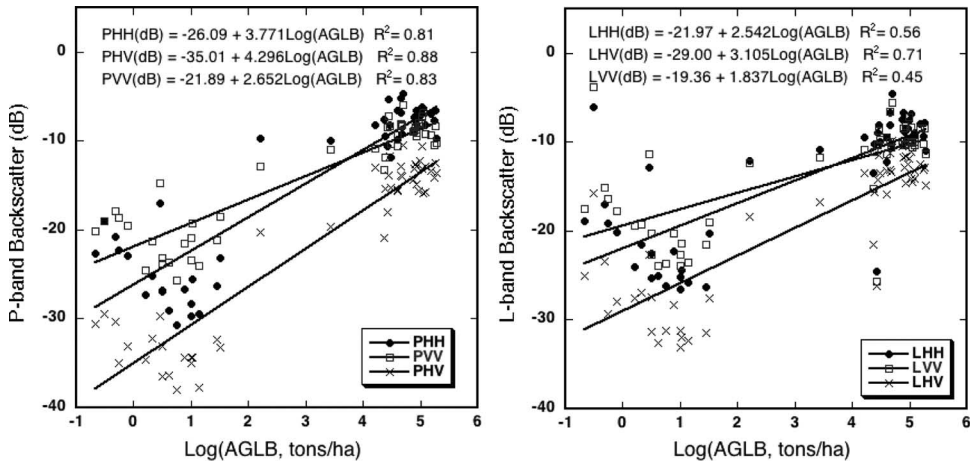


Fig. 7. Backscattering coefficient at linear polarization combinations versus the natural logarithm of field-measured AGLB for 64 stands including forests and other nonforest vegetation types.

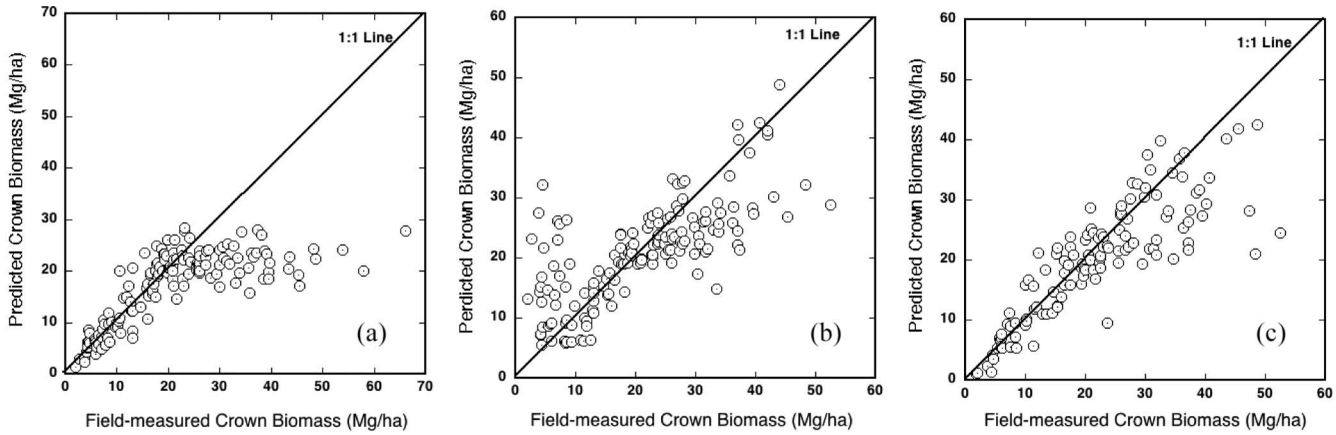


Fig. 8. Field-measured versus predicted crown biomass in megagrams per hectare from (a) L-band ($R^2 = 0.54$, $P$-value $< 0.0001$), (b) P-band ($R^2 = 0.55$, $P$-value $< 0.0001$), and (c) combined L-band and P-band ($R^2 = 0.73$, $P$-value $< 0.0001$). Line shows 1 : 1 relationship.

### *B. Estimation of Crown and Stem Biomass*

Estimation of crown biomass was performed using (3). Here, by crown biomass, we refer to both the biomass of the forest tree crown and the biomass of nonforest vegetation such as the sagebrush. The backscatter data were extracted for all plot locations within the 10-m resolution SAR images ($n = 623$) and were used in bootstrapping and holdout procedure, discussed in Section V, to estimate the coefficients of (3) at L-band and P-band frequencies (Table III). The comparison of field-measured and predicted biomass values is given in Fig. 8(a) and (b), respectively, for L-band and P-band. The estimation provided similar results at both frequencies, $R^2 = 0.54$ for L-band and $R^2 = 0.55$ for P-band. However, the noticeable difference was the pattern of the points spread around the $1:1$ line. The L-band results showed a very close correlation at lower biomass values and almost no correlation at high crown biomass values. This was expected because the attenuation of the L-band signal increased when the density of foliage and branches increased in tree crowns, reducing the L-band sensitivity to high crown biomass.

The P-band result, however, showed an opposite pattern, with larger spread of points at low biomass values. For areas of low biomass density such as early successional forests and sagebrush, the P-band backscatter is very sensitive to soil surface and subsurface conditions. The overestimation of crown biomass for low-density vegetation is primarily due to the higher backscatter returns from the subsurface soil layers (moisture and texture gradients), similarly observed in Fig. 7. A close examination of both results suggested that a combination of L-band and P-band data for, respectively, the low and high biomass values would probably produce the best accuracy for crown biomass estimation. By using only cross-polarized backscatter in L-band and P-band and a quadratic form as in (3), we developed a new algorithm with the general expression

$$\log(W_c) = a_0 + a_1 \text{LHV}\,\cos(\theta_0 - \theta_l) + a_2\,(\text{LHV}\,\cos(\theta_0 - \theta_l))^2 + b_1 \text{PHV}\,\cos(\theta_0 - \theta_l) + b_2\,(\text{PHV}\,\cos(\theta_0 - \theta_l))^2. \tag{7}$$

The coefficients for (7) are estimated using similar approach and are provided in Table III. The result from the new algorithm is shown in Fig. 7. The comparison with the field-measured data produced an improved $R^2 = 0.73$ ($P < 0.00001$), with standard root mean square error (RMSE) of 1.87 Mg/ha, and with points spreading more evenly around the $1:1$ line.

TABLE III
COEFFICIENTS OF THE ESTIMATION ALGORITHM FOR CROWN AND STEM BIOMASS DERIVED FROM MULTIVARIATE NONLINEAR REGRESSION ANALYSIS

| Biomass Components Log (Mg/ha) | Frequency Band | $a_0$ | $a_1$ | $a_2$ | $b_1$ | $b_2$ | $c_1$ | $c_2$ |
|---|---|---|---|---|---|---|---|---|
| Crown | P-band | 6.215 | 0.058 | -0.0017 | 0.192 | 0.0098 | 0.0962 | -0.0028 |
| Crown | L-band | 7.496 | 0.664 | 0.0084 | 0.017 | -0.0016 | -0.322 | 0.000007 |
| Crown | LHV, PHV | 4.784 | 0.0931 | 0.0012 | 0.0538 | 0.00034 | - | - |
| Stem | P-band | 8.104 | 0.112 | -0.0018 | 0.396 | 0.0143 | -0.131 | -0.0081 |
| Stem | L-band | 9.184 | 0.769 | 0.0085 | 0.188 | 0.0002 | -0.165 | -0.0038 |

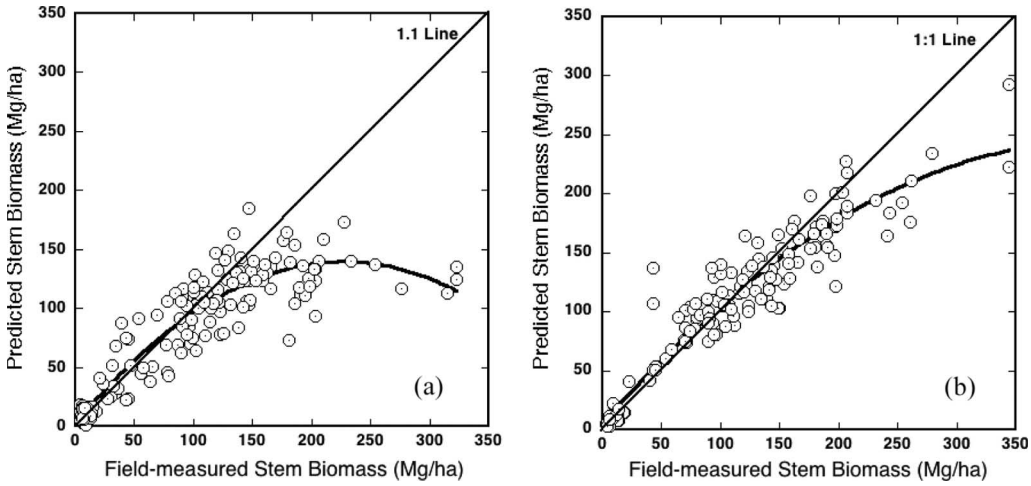


Fig. 9. Field-measured versus predicted stem biomass in megagrams per hectare from (a) L-band ($R^2 = 0.57$, $P$-value $< 0.0001$) and (b) P-band ($R^2 = 0.81$, $P$-value $< 0.0001$). Line shows $1:1$ relationship.

For stem biomass, we estimated the unknown coefficients in (4) using a similar approach and the extracted L-band and P-band backscatter data from the plot locations. In this analysis, we included only the forest plots (427 plots from 42 stands) where data on the stem biomass were available. The coefficients are provided in Table III. Following similar analysis as in estimating the crown biomass, we calculated the average unbiased estimation of accuracy from the bootstrapping approach. As expected, the P-band data provided better accuracy ($\mathrm{R}^2 = 0.81$; RMSE $= 11.3$ Mg/ha) than L-band ($\mathrm{R}^2 = 0.57, 19.7$ Mg/ha). Fig. 9 shows the prediction of stem biomass from both bands and the spread of the data around a $1:1$ line representing an ideal estimation. These figures were compiled using all forest plots including early successional forests. The estimation errors associated with these plots are greater than the mean error due to the degraded sensitivity of P-band measurements to low biomass values. By eliminating plots representing biomass values less than 20 Mg/ha, we were able to improve the estimation error by more than 10%. This result suggests that the best region for P-band biomass estimation is for forests above 20 Mg/ha.

The performance of the L-band and P-band estimation algorithms degraded after approximately 100 and 200 Mg/ha of biomass, respectively, when the radar measurements increasingly lost their sensitivity to biomass increments. Further examination of biomass prediction at plot locations suggested that the performance of the algorithm also degraded over areas at higher elevation and steeper slopes. For these areas, the backscattering mechanisms from tree stems were more complex, and the scattering contributions at different polarizations were not well represented by the geometrical relations given in (4). The overall accuracy from the P-band estimation was satisfactory and could not be improved much further by combining L-band and P-band data as in the crown estimation approach.

### C. Spatial Distribution of Stem and Crown Biomass

The application of crown and stem biomass algorithms on SAR images can produce spatial distribution of these continuous variables over the entire image area. However, to produce maps that can be more readily used by fire managers, we designed a classification approach to convert the estimated biomass components, estimated in logarithmic values to actual biomass range classes. Classes were assigned to biomass ranges by simply applying thresholds to the estimated biomass values. The thresholds were selected based on the biomass ranges and the expected accuracy, resulting in finer class intervals for low biomass values and larger intervals for high biomass values. The accuracy of the classified maps was almost equal to the estimation accuracy for logarithm of biomass and in general were higher than the accuracy if the actual biomass values were mapped. The thresholds for biomass classes covered, to a large extend, the errors associated with transforming the estimated values from logarithmic values to actual biomass. Fig. 10 shows the classified biomass images for an area centered on the Lamar Valley and the Soda Butte in the northwestern part of the park. The overall accuracy of classification was determined using

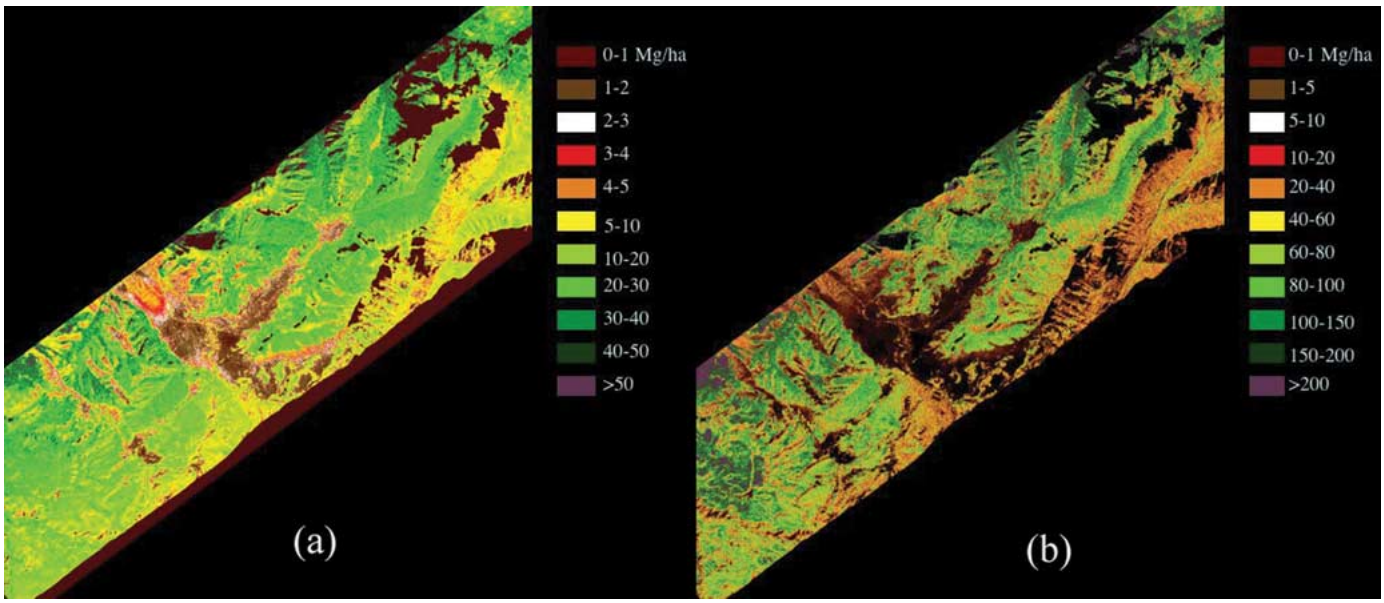


Fig. 10. Distribution of crown and stem biomass over the Lamar Valley and Soda Butte area in northeastern YNP. (a) Crown live biomass in megagrams per hectare with classification accuracy of 84%. (b) Stem live biomass in megagrams per hectare with classification accuracy of 86%.

the standard error matrix, which resulted in 84% and 86% accuracies for crown and stem classes, respectively.

### D. Estimation of Canopy Fuel Weight

Radar backscatter responds to live biomass, and the results above demonstrate the retrieval of crown live biomass. However, crown fires propagate through and consume both live and dead canopy biomass, and this combined fuel load is what is commonly used in fire modeling. Using the field-measured dead canopy biomass, the crown biomass was converted to total fuel weight by adjusting the values for the dead biomass using a linear regression model ($W_{\rm tcf} = 0.125 + 1.108\ W_c$, $R^2 = 0.995$), where $W_{\rm tcf}$ is the total canopy fuel, and $W_c$ is the radar-derived crown biomass. The model is developed by a randomly sampled data point from the forest plots. On average, the dead material constitutes less than 10% of the total canopy fuel that varies depending on the forest type and successional stage. After conversion to canopy fuel, we reexamined the accuracy of the results by cross validating the radar-derived canopy fuel with the remaining plot data $(n = 177)$ not used in the development of the regression model. The coefficient of determination was $R^2 = 0.85$, and the cross-validated RMSE was 1.7 Mg/ha. From the total canopy fuel, additional information such as 1-h and 10-h branchwood fuels can be readily estimated. These variables, although derived from allometric equations based on forest structure, are closely correlated with the total canopy fuel weight and are important in understanding and predicting the fire intensity and spread [5], [21]. The radar-derived crown biomass was converted using regression models based on a randomly sampled plot data. The estimated values were cross validated with the remaining plot data $(n = 199)$ and showed coefficient of determination of $R^2 = 0.83$ and $R^2 = 0.87$, respectively, for 1-h and 10-h branchwood fuel loads (Fig. 11).

### E. Estimation of Canopy Bulk Density

Equation (6) was used to compute the canopy bulk density (or crown bulk density) from the field-measured forest structure assuming uniform canopy distribution along the canopy height. This variable is strongly correlated with the canopy height. However, height was not estimated from the AIRSAR polarimetric data. From the field data, we examined the relationship between crown and stem weight with canopy bulk density, and in both cases, the individual correlations were not very high ($R^2 = 0.34$ with crown biomass and $R^2 = 0.21$ with stem biomass). However, by transforming the bulk density and stem and crown biomass to natural logarithm to stabilize the variance and account for the nonlinearity in the relationship, we were able to develop a linear regression model between the bulk density and crown and stem biomass in the form

$$\ln(\mathrm{CBD}) = a_0 + a_1 \ln(W_c) + a_2 \ln(W_s) \tag{8}$$

where $a_0 = -1.755$, $a_1 = 1.895$, and $a_2 = -0.891$. Like all the previous cases, the regression model is developed from randomly selected plot data. We used the above relationship on the radar estimation of crown and stem biomass and cross validated the canopy bulk density with the remaining plot data. The result is shown in Fig. 12. The use of stem and crown biomass together provided for more than 80% of the CBD variations ($R^2 = 0.85$, $P < 0.00001$). The cross-validated RMSE of the CBD estimation on the logarithmic scale was approximately 0.67 kg/m$^3$.

### F. Estimation of Foliage Biomass

Using 100% moisture content, we were able to estimate the foliage biomass or dry biomass directly from the crown biomass estimation. From a randomly selected plot data $(n = 271)$, we developed a linear model ($W_f = -0.5523 + 0.3856 W_c$,

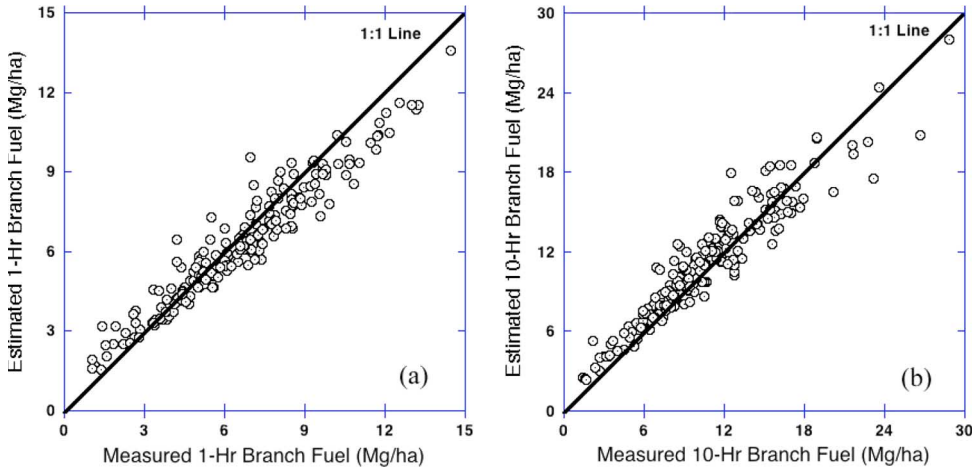


Fig. 11. Field-based versus radar-derived canopy branchwood fuels (with 1 : 1 line shown). (a) 1-h fuel weight in megagrams per hectare ($R^2 = 0.83$, $P < 0.00001$, RMSE $= 0.92$ Mg/ha). (b) 10-h fuel weight in megagrams per hectare ($R^2 = 0.87$, $P < 0.00001$, RMSE $= 1.6$ Mg/ha).

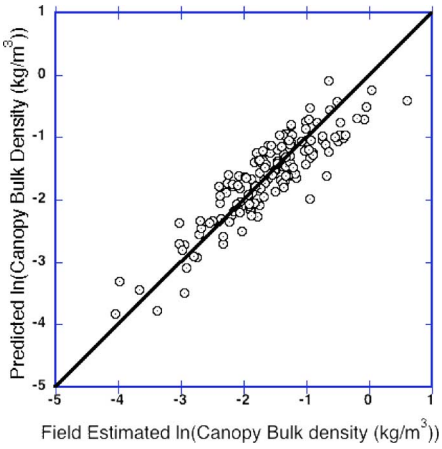


Fig. 12. Field-estimated versus radar-predicted canopy bulk density in kilograms per cubic meter (log transformed) ($R^2 = 0.85$, $P < 0.00001$, RMSE $=$ 0.67 kg/m$^3$).

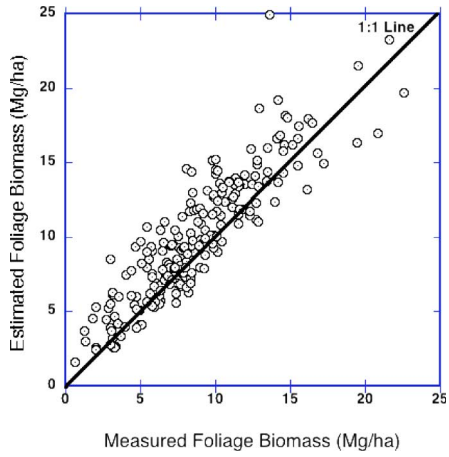


Fig. 13. Field-measured versus radar-estimated foliage biomass in megagrams per hectare ($R^2 = 0.78$, $P < 0.00001$, RMSE $= 1.8$ Mg/ha). Line shows 1 : 1 relationship.

$R^2 = 0.91$) between crown and foliage biomass that was used to estimate foliage biomass from the radar-derived crown biomass for the AIRSAR image. The estimation was cross validated with the plot data not used in developing the regression model ($n = 150$), and the prediction had $R^2 = 0.78$ ($P < 0.00001$) and RMSE $= 1.8$ Mg/ha (Fig. 13).

## VII. Summary and Discussion

Polarimetric and interferometric SAR data were analyzed to examine whether the sensitivity of radar backscatter measurements to vegetation structure and biomass can be used to estimate forest fire fuel parameters. We chose the YNP as the study area and the airborne multifrequency SAR polarimetric measurements at L-band and P-band and the interferometric estimation of surface topography at C-band to perform the analysis. The results in this paper indicate that simple semi-empirical models have the potential to predict canopy fuel parameters with accuracy suitable for forest fire models and management approaches. The overall assessment of the models also suggested that P-band polarimetric data provided more accurate estimates of fuel components, in particular over old-growth forests with developed fuel loads. Whereas fuel loads for shrubs and low-density forests were estimated with higher accuracy using L-band data. The best performance was achieved when L-band and P-band HV polarizations were combined to estimate the crown biomass and subsequently the total canopy fuel weight over the entire range of fuel loads available in the park. The estimation of crown and stem biomass when compared with the field measurements at the plot level resulted in $R^2 > 0.7$ and with RMSE errors of 1.87 and 11.3 Mg/ha, respectively, for crown and stem biomass. The classification of the biomass to range classes produced accuracies larger than 80% as high biomass values with largest errors were all lumped in a few classes. The development of the model and the process of estimating the fuel load provided the following conclusions.

1) There are a number of discrepancies between the backscatter measurements of forest biomass and the forest structure measured at plot level. Although reasonable correlations were found between radar backscatter measurements and the biomass components, the accuracy of plot locations, the errors associated with the allometric equations, and the speckle noise in radar images

introduced a significant source of variability in the estimated results. Stand-level data that resulted in averaging and extrapolating plot data over larger areas reduced the errors in field-based biomass components, errors due to misregistration, and speckle noise, and improved the correlations with the radar backscatter measurements.

2) The radar backscatter measurements in decibels were correlated with the logarithm of biomass components. This introduced another source of error when transforming the biomass components estimated in logarithmic scale to actual biomass values. In this paper, the accuracy in stem and crown biomass estimation and the RMSE were all computed and reported in logarithmic values. The actual biomass values were then classified in biomass ranges that incorporated the errors associated with transforming the results from logarithmic to actual values. The final spatial distributions of biomass and canopy fuel components were produced in classified form and with biomass ranges suitable for wildfire simulation models.
3) Another possible source of error in directly estimating AGLB values from radar data is the discrepancy between the radar sensitivity to wet aboveground biomass and the field-measured dry biomass from allometric equations. The dielectric constant and the moisture content of biomass components (leaves, branches, and stems) impact the radar backscatter measurements and introduce larger variability when compared with dry biomass. In experiments that moisture content is included in the field measurements and incorporated in the radar data analysis, the biomass estimation is improved [14].
4) Canopy fuel parameters such as the bulk density require direct measurements of canopy height and canopy base height. These parameters are difficult to measure in the field in particular over complex terrains. In this paper, we employed an indirect approach by developing a regression model between the crown and stem biomass and the bulk density. Although a reasonable accuracy was found with the plot-level data, mainly located in areas with low relief, the spatial accuracy of the results was probably reduced over areas with high relief. In fact, the accuracy for all fuel parameters estimated in this paper was assessed only with plot data, and no independent assessment of the spatial accuracy of the results over the entire area covered by radar images was performed.
5) In areas with large topographical variations such as the YNP, accurate estimations of surface elevation and slopes are needed to correct the backscatter measurements and improve the biomass estimation by modifying the contribution of scattering mechanisms as in (3), (4), and (7). In such landscapes, direct estimation by linear regression approaches may introduce large errors in the predicted biomass components from SAR images. Inclusion of surface elevation acquired by interferometric sensors along with the polarimetric data has dramatically improved the results in this paper.
6) Variations in surface characteristics such as soil moisture and roughness impact both the radar backscatter measurements and the retrieval of vegetation structure. We have reduced the impact of these parameters in biomass estimation by using a semiempirical approach. Determination of unknown coefficients in (7) using radar data will calibrate the equations for the moisture and roughness values of the surface. In general, this process will result in a site-specific estimation algorithm for forest biomass components. The errors associated with differences in soil moisture and surface roughness parameters of different stands and plots will be reflected in the overall estimation errors. However, we expect the impact of surface parameters to be small for various reasons: the algorithm is strongly dependent on the cross-polarized HV term, which is less sensitive to surface parameters, and for forests with high biomass density, the backscatter values are less sensitive to surface parameters because of the attenuation of the radar signal before reaching the surface. Further study is required to accurately quantify the effects of surface parameters to the estimation algorithm.

Our results suggest that crown biomass and height are the most important structural variables to estimate forest canopy fuel loads. Polarimetric SAR data at longer wavelengths such as P-band provide a more accurate estimate of crown biomass in particular for medium to dense forest fuels. Saturation of the radar signal at shorter wavelength due to attenuation through the foliage and the crown layer is the main reason for the better performance of P-band data versus L-band. For other parameters such as canopy height, accurate estimates can be achieved either by radar interferometry [13] or laser altimetry by lidar sensors [11]. This conclusion introduces a new area of research for wildfire applications rarely discussed in the radar remote sensing literature. In most forestry applications of radar remote sensing, the emphasis has been on the estimation of the total AGLB [14], [24], [25].

We expect that the general form of the algorithm introduced in this paper be applicable for other regions and forest types. In general, the application of the algorithm with the same coefficients will provide the distribution of relative fuel loads across the landscape and forest types for any region. However, for the absolute accuracy, the algorithm must be calibrated using radar images and few forest plots acquired over the new region.

The results from this paper also suggest that spaceborne polarimetric radar measurements at longer wavelengths (P-band) can be used as a potential tool for forest fire management. Different classes of canopy fuel components, such as the ones produced in this paper, can be readily integrated in different forest fire models. The high spatial resolution of radar images and the all-weather data collection provide additional capability for monitoring areas with potential fire hazards, areas under the fire, and the area and intensity of the postfire disturbance.

## ACKNOWLEDGMENT

This work was partially carried out at the Jet Propulsion Laboratory, California Institute of Technology, under a contract with the National Aeronautics and Space Administration. The SAR data acquisition and analysis and the field data collection and analysis were under a contract with the Yellowstone

Ecological Research Center and was partially performed at the Institute of Environment, University of California at Los Angeles.

## REFERENCES


[1] "FRA global forest fire assessment 1990–2000," *Forest Resources Assessment Programme*, 2001, Rome, Italy: FAO. Working Paper 55.

[2] C. Carmona-Moreno, A. Belward, J. P. Malingreau, A. Hartley, M. Garcia-Algere, M. Antonovskiy, V. Buchshtaber, and V. Pivovarov, "Characterizing interannual variations in global fire calendar using data from Earth observing satellites," *Glob. Chang. Biol.*, vol. 11, no. 9, pp. 1537–1555, Sep. 2005.

[3] M. O. Andreae, "Biomass burning: Its history, use, and distribution and its impact on environmental quality and global climate," in *Global Biomass Burning, Atmospheric, Climatic and Biosphere Implication*, J. S. Levine, Ed. Cambridge, MA: MIT Press, 1991, pp. 3–21.

[4] M. A. Finney, *FARSITE: Fire Area Simulator-Model Development and Evaluation*. Ogden, UT: Dept. Agriculture, Forest Service Rocky, Mountain Res. Station, 1998. Research Paper RMRS-RP-4, 47 pp.

[5] J. H. Scott and E. D. Reinhardt, *Assessing Crown Fire Potential by Linking Models of Surface and Crown Fire Behavior*. Fort Collins, CO: USDA Forest Service, Rocky Mountain Res. Station, 2001. Research Paper RMRS-RP-29.

[6] D. P. Roy, Y. Jin, P. E. Lewis, and C. O. Justice, "Prototyping a global algorithm for systematic fire-affected area mapping using MODIS time series data," *Remote Sens. Environ.*, vol. 97, no. 2, pp. 137–162, Jul. 2005.

[7] J. T. Morisette, L. Giglio, I. Csiszar, and C. O. Justice, "Validation of the MODIS active fire product over southern Africa with ASTER data," *Int. J. Remote Sens.*, vol. 26, no. 19, pp. 4239–4264, Oct. 2005.

[8] C. O. Justice, L. Giglio, S. Korontzi, J. Owens, J. Morisette, D. P. Roy *et al.*, "The MODIS fire products," *Remote Sens. Environ.*, vol. 83, no. 1/2, pp. 244–262, 2002.

[9] J. Epting, D. Verbyla, and B. Sorbel, "Evaluation of remotely sensed indices for assessing burn severity in interior Alaska using Landsat TM and ETM," *Remote Sens. Environ.*, vol. 96, no. 3/4, pp. 328–339, Jun. 2005.

[10] J. V. Wagtendonk, R. R. Root, and C. H. Key, "Comparison of AVIRIS and Landsat ETM + detection capabilities for burn severity," *Remote Sens. Environ.*, vol. 92, no. 3, pp. 397–408, Aug. 2004.

[11] H.-E. Andersen, R. J. McGaughey, and S. E. Reutebuch, "Estimating forest canopy fuel parameters using LIDAR data," *Remote Sens. Environ.*, vol. 94, no. 4, pp. 441–449, Feb. 2005.

[12] R. Dubayah and J. B. Drake, "Lidar remote sensing for forestry," *J. For.*, vol. 98, no. 6, pp. 44–46, Jun. 2000.

[13] H.-E. Andersen, R. J. McGaughey, S. E. Reutebuch, G. F. Schreuder, J. Agee, and B. Mercer, "Estimating canopy fuel parameters in a Pacific Northwest conifer forest using multifrequency polarimetric IFSAR," in *Proc. 20th Congr. Int. Soc. Photogramm. Remote Sens.*, Istanbul, Turkey, Jul. 12–23, 2004, vol. 35, pt. B.

[14] S. Saatchi and M. Moghaddam, "Estimation of crown and stem water content and biomass of boreal forest using polarimetric SAR imagery," *IEEE Trans. Geosci. Remote Sens.*, vol. 38, no. 2, pp. 697–709, Mar. 2000.

[15] D. G. Despain, *Yellowstone Vegetation: Consequences of Environment and History in a Natural Setting*. Santa Barbara, CA: Roberts Rinehart Publishers, 1990.

[16] W. H. Romme and D. G. Despain, "Historical perspective on the yellowstone fires of 1988," *BioScience*, vol. 39, no. 10, pp. 695–699, 1989.

[17] W. H. Romme, "Fire and landscape diversity in subalpine forests of Yellowstone National Park," *Ecol. Monogr.*, vol. 52, no. 2, pp. 199–221, 1982.

[18] M. E. Jakubauskas, "Thematic Mapper characterization of lodgepole pine seral stages in Yellowstone National Park, USA," *Remote Sens. Environ.*, vol. 56, no. 2, pp. 118–132, May 1996.

[19] D. M. Debinski, K. Kindscher, and M. E. Jakubauskas, "A remote sensing and GIS-based model of habitats and biodiversity in the Greater Yellowstone ecosystem," *Int. J. Remote Sens.*, vol. 20, no. 17, pp. 3281–3291, Nov. 1999.

[20] R. Daubernmire, "Forest vegetation of northern Idaho and adjacent Washington, and its bearing on concepts of vegetation classification," *Ecol. Monogr.*, vol. 22, no. 4, pp. 301–330, 1952.

[21] J. K. Brown, "Weight and density of crowns of Rocky Mountain Conifers," USDA For. Serv. Res, Ogden, UT, 1978. Pap. INT-197.

[22] J. K Brown, R. D. Oberheu, and M. Cameron, "Handbook for inventorying surface fuels and biomass in the interior West. Gen.," Dept. Agriculture, Forest Service, Intermountain Forest and Range Experiment Station, Ogden, UT, Tech. Rep. INT_129, 1982. 48 p.

[23] D. D. Van Hooser and D. C. Chojnacky, "Whole tree volume estimates for the Rocky Mountain States," Dept. Agriculture, Forest Service, Intermountain Forest and Range Experiment Station, Ogden, UT, 1983. Res. Bull. INT_29, 69 p.

[24] C. Dobson, F. Ulaby, L. Pierce, T. Sharik, K. Bergen, J. Kellndorfer, J. R. Kendra, E. Li, Y. C. Lin, A. Nashashibi, K. Sarabandi, and P. Siqeira, "Estimation of forest biomass characteristics in northern Michigan with SIR-C/X-SAR data," *IEEE Trans. Geosci. Remote Sens.*, vol. 33, no. 4, pp. 877–894, July 1995.

[25] T. Le Toan, A. Beaudoin, J. Riom, and D. Guyon, "Relating forest biomass to SAR data," *IEEE Trans. Geosci. Remote Sens.*, vol. 30, no. 2, pp. 403–411, Mar. 1992.

[26] M. Moghaddam and S. Saatchi, "Monitoring tree moisture using an estimation algorithm applied to SAR data from BOREAS," *IEEE Trans. Geosci. Remote Sens.*, vol. 37, no. 2, pp. 901–916, Mar. 1999.

[27] L. Tsang, Z. Chen, S. Oh, R. J. Marks, II, and A. T. C. Chang, "Inversion of snow parameters from passive microwave remote sensing measurement by a neural network trained with a multiple scattering model," *IEEE Trans. Geosci. Remote Sens.*, vol. 30, no. 5, pp. 1015–1024, Sep. 1992.

[28] F. Del Frate, P. Ferrazzoli, and G. Schiavon, "Retrieving soil moisture and agricultural variables by microwave radiometry using neural networks," *Remote Sens. Environ.*, vol. 84, no. 2, pp. 174–183, Feb. 2004.

[29] S. Saatchi and K. McDonnald, "Coherent effects in microwave backscattering models for forest canopies," *IEEE Trans. Geosci. Remote Sens.*, vol. 35, no. 4, pp. 585–598, Jul. 1997.

[30] R. Lang, "Scattering from a layer of discrete random medium over a random interface: Application to microwave backscattering from forests," *Waves Random Media*, vol. 14, no. 2, pp. S359–S391, 2004.

[31] E. J. Rignot, R. Zimmermann, and J. J. van Zyl, "Spacebome applications of p Band imaging radars for measuring forest biomass," *IEEE Trans. Geosci. Remote Sens.*, vol. 33, no. 5, pp. 1162–1169, Sep. 1995.

[32] J. J. van Zyl, "The effects of topography on the radar scattering from vegetated areas," *IEEE Trans. Geosci. Remote Sens.*, vol. 31, no. 1, pp. 153–160, Jan. 1993.

[33] S. Saatchi, R. Houghton, R. Avala, Y. Yu, and J.-V. Soares, "Spatial distribution of live aboveground biomass in the Amazon Basin," *Glob. Chang. Biol.*, vol. 13, pp. 816–837, 2007.

[34] M. B. Steele, J. C. Winne, and R. L. Redmond, "Estimation and mapping of misclassification probabilities for thematic land cover types," *Remote Sens. Environ.*, vol. 66, no. 2, pp. 192–202, Nov. 1998.

[35] K. S. Fassnacht, S. T. Gower, M. Norman, and R. E. A. McMurtrie, "Comparison of optical and direct methods for estimating foliage surface area index in forests," *Agric. For. Meteorol.*, vol. 71, no. 1/2, pp. 183–207, 1994.

[36] R. E. Keane, E. D. Reinhardt, J. Scott, K. Gray, and J. Reardon, "Estimating forest canopy bulk density using six indirect methods," *Can. J. For. Res.*, vol. 35, no. 3, pp. 724–739, Mar. 2005.

[37] D. A. Roberts, P. E. Dennison, M. Morais, M. E. Gardner, J. Regelbrugge, and S. L. Ustin, "Mapping wildfire fuels using imaging spectrometry along the wildland urban interface," in *Proc. Joint Fire Sci. Conf. Workshop*, Boise, ID, Jun. 17–19, 1999, vol. 1, pp. 212–223.

[38] J. B. Drake, R. O. Dubayah, R. G. Knox, D. B. Clark, and J. B. Blair, "Sensitivity of large footprint lidar to canopy structure and biomass in a neotropical rainforest," *Remote Sens. Environ.*, vol. 81, no. 2/3, pp. 378–392, Aug. 2002.

[39] J. Askne, M. Santoro, G. Smith, and J. Fransson, "Multitemporal repeat pass SAR interferometry of boreal forests," *IEEE Trans. Geosci. Remote Sens.*, vol. 41, no. 7, pp. 1540–1550, Jul. 2003.

[40] D. Riano, E. Chuveico, J. Salas, A. Palacio-Orueta, and A. Bastarrika, "Generation of fuel type maps from Landsat-TM images and auxiliary data in Mediterranean ecosystems," *Can. J. For. Res.*, vol. 32, no. 8, pp. 1301–1315, 2002.

[41] D. A. Roberts, P. E. Dennison, S. Peterson, S. Sweeney, and J. Rechel, "Evaluation of AVIRIS and MODIS measures of live fuel moisture and fuel condition in a shrubland ecosystem in southern California," *J. Geophys. Res.*, vol. 111, 2006. G04S02, DOI:10.1029/2005JG000113.

[42] P. E. Dennison, D. A. Roberts, S. H. Peterson, and J. Rechel, "Use of normalized difference water index for monitoring live fuel moisture," *Int. J. Remote Sens.*, vol. 26, no. 5, pp. 1035–1042, 2005.

[43] E. Chuveico, D. Riano, I. Aguado, and D. Cocero, "Estimation of fuel moisture content from multitemporal analysis of Landsat-TM reflectance data: Applications in fire danger assessment," *Int. J. Remote Sens.*, vol. 23, no. 11, pp. 2145–2162, 2002.

[44] E. Chuvieco, I. Aguado, D. Cocero, and D. Riano, "Design of an empirical index to estimate fuel moisture content from NOAA-AVHRR analysis in

forest fire danger studies," *Int. J. Remote Sens.*, vol. 24, no. 8, pp. 1653–1668, 2003.
[45] D. Riano, E. Chuveico, S. Condes, J. Gonzalez-Matesanz, and S. L. Ustin, "Generation of crown bulk density for Pinus sylvestris L. from lidar," *Remote Sens. Environ.*, vol. 92, no. 3, pp. 345–352, Aug. 2004.
[46] D. Riano, E. Meier, B. Allgower, E. Chuveico, and S. L. Ustin, "Modeling airborne laser scanning data for the spatial generation of critical forest parameters in fire behavior modeling," *Remote Sens. Environ.*, vol. 86, no. 2, pp. 177–186, Jul. 2003.
[47] D. Despain, A. Rodman, P. Schullery, and H. Shovic, "Burned area survey of Yellowstone National Park, Wyoming, Montana, Idaho," in *The Fires of 1988*. Wyoming, ID: Division Res. Geographic Inf. Syst. Lab. Yellowstone Nat. Park, 1989.
[48] S. Saatchi, J. van Zyl, and G. Assrar, "Estimation of canopy water content in Konza prairie grasslands using synthetic aperture radar measurements during FIFE," *J. Geophys. Res.*, vol. 100, no. D12, pp. 25481–25496, 1995.
[49] W. H. Press, B. P. Flannery, S. A. Teukolsky, and W. T. Vettering, *Numerical Recipes: The Art of Scientific Computing*. New York: Cambridge Univ. Press, 1989.
[50] R. A. Hartford and R. C. Rothermel, "Fuel moisture as measured and predicted during the1988 fires in Yellowstone Park," Dept. Agriculture Forest Service Intermountain Forest and Range Experiment Station, Ogden, UT, 1991. Res. Note INT-396.
[51] C. W. Philpot and R. W. Mutch, "the seasonal trend in moisture content, ether extractives, and energy of Ponderosa Pine and Douglas-Fir Needles," Dept. Agriculture Forest Service Intermountain Forest and Range Experiment Station, Ogden, UT, 1971. Res. Pap. INT_112.

**Sassan Saatchi** (S'85–M'88) received the B.S. and M.S. degrees in electrical engineering from the University of Illinois, Chicago, in 1981 and 1983, respectively, and the Ph.D. degree from George Washington University, Washington, DC, in 1988. His Ph.D. thesis was on the concentration in electrophysics and modeling of wave propagation in natural media.

From 1989 to 1991, he was a Postdoctoral Fellow with the National Research Council and was with the Laboratory for Terrestrial Physics, NASA/Goddard Space Flight Center, working on the hydrological application of active and passive microwave remote sensing. Since April 1991, he has been with the Radar Science and Engineering Section, Jet Propulsion Laboratory, California Institute of Technology, Pasadena, where, as a Scientist, he is involved in developing microwave scattering and emission models for soil and vegetated surfaces and retrieval algorithms for estimating biophysical parameters from spaceborne remote sensing instruments. He has been a Principal or Co-Investigator in several interdisciplinary international projects such as FIFE, EFEDA, Magellan, Mac-Hydro, Hapex-Sahel, BOREAS, LCLUC, and LBA. His present research activities include biomass and soil surface moisture estimation in different ecosystems, land use and land cover change, forest regeneration monitoring over tropical rain forests, and ecological modeling of species range distribution and biodiversity using remote sensing. His research interests also include wave propagation in disordered/random media and EM scattering theory. He has been involved in developing and teaching courses in the use of remote sensing for environmental problems.

**Kerry Halligan** received the B.S. degree in ecology from Western Washington University, Bellingham, in 1996 and the M.A. degree in geography from the University of California (UC), Santa Barbara, in 2002. He is currently working toward the Ph.D. degree in geography at UC Santa Barbara, where his research focuses on mapping vegetation type, structure, and conditions in Yellowstone National Park.

Since 1997, he has been a Research Scientist with the Yellowstone Ecological Research Center, Bozeman, MT. His research interests include applications of multispectral, hyperspectral, and lidar data for mapping of vegetation functional types, forest biophysical parameters including carbon stocks and wildfire fuels, invasive species, and vegetation change in response to disturbance and climate change.

**Don G. Despain** received the B.S. degree in botany from the University of Wyoming, Laramie, in 1966, the M.S. degree from the University of Arizona, Tucson, in 1967, and the Ph.D. degree from the University of Alberta, Edmonton, AB, Canada, in 1971.

From late 1971 to 1993, he was with Yellowstone National Park. In 1993, he joined the U.S. Geological Survey, Bozeman, MT, where he continued his work in vegetation mapping, fire behavior and ecology, and range ecology. He retired in January 2006 but is continuing his studies on an *ad hoc* basis, concentrating on willow ecology.

**Robert L. Crabtree** received the B.S. and Ph.D. degrees in forestry, wildlife, and range sciences from the University of Idaho, Moscow, and the M.S. degree from Utah State University, Logan.

In 1989, he was a Visiting Scholar (postdoctoral position) with the University of California, Berkeley, working on wildlife survey methods and animal movements models. In 1993, he founded a nonprofit organization dedicated to long-term large-scale ecological research in the Yellowstone region. He is currently with the Yellowstone Ecological Research Center, Bozeman, MT. He is an affiliate faculty at numerous universities and his research focuses on predator–prey relations, landscape ecology, and remote sensing applications to vegetation dynamics and species distributions.